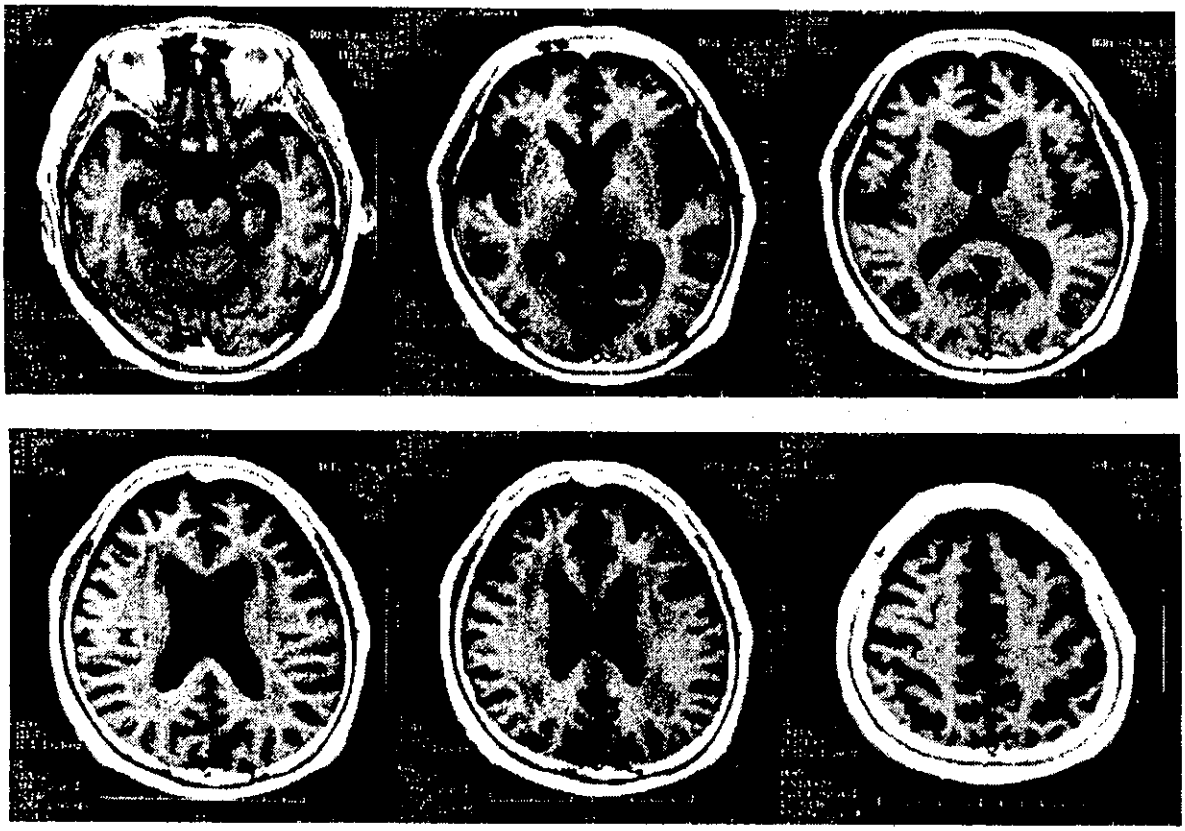

図1　T_1-WI

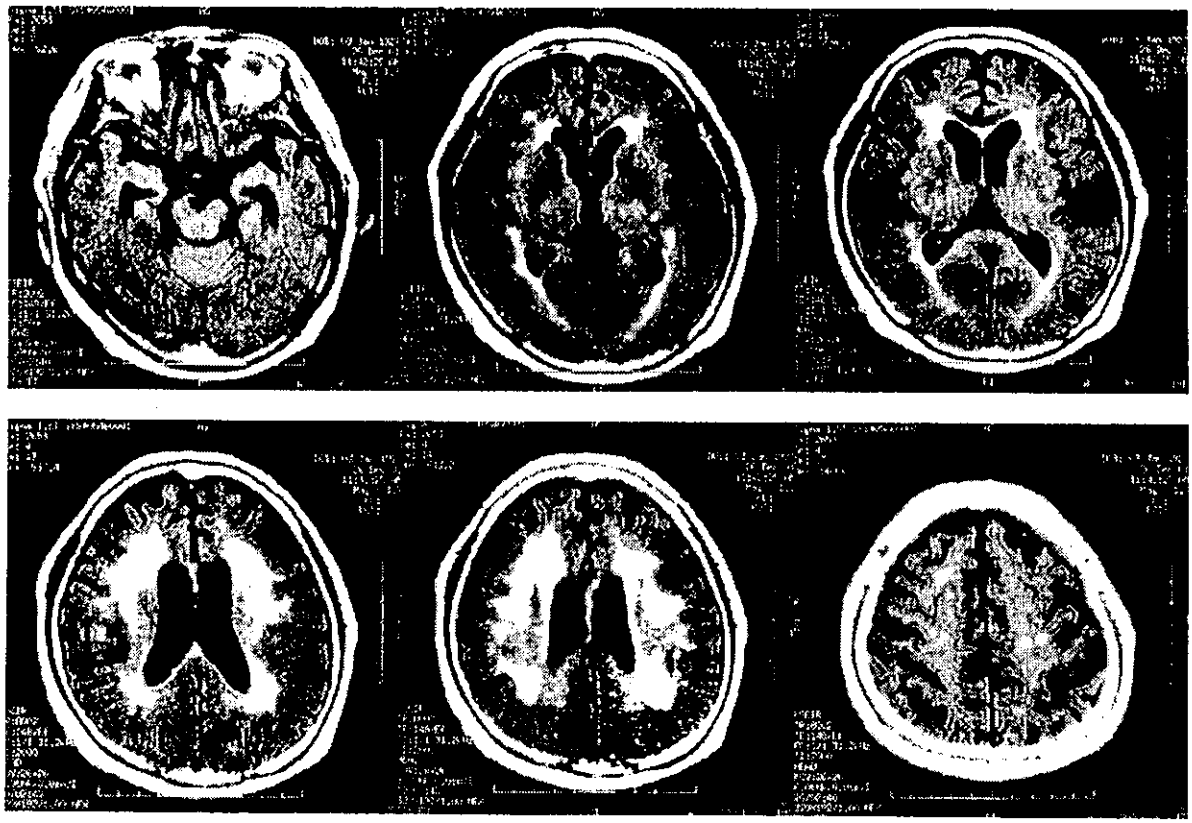

図2　FLAIR

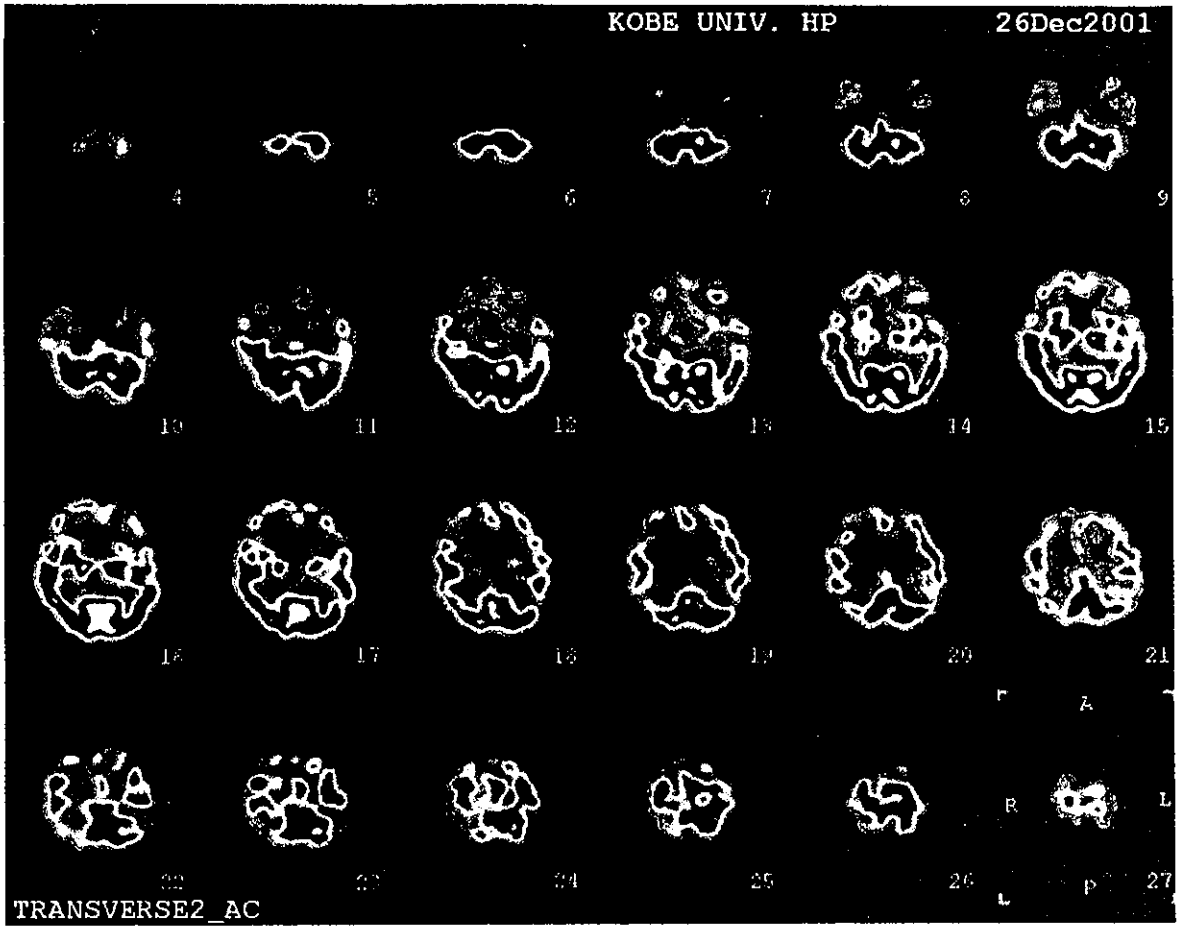

図3　IMP-SPECT

神経心理テスト：抑うつ傾向が認知機能に及ぼす影響を検討するため，マレイン酸フルボキサミンを3カ月間投与した．投与後，MMS，HDS-Rを再検したが，それぞれ22点，HDS-R 22点でありほとんど変化はみられなかった．CDRは0.5．WAIS-RではVIQ 93，PIQ 83，IQ 87であり，動作性知能に低下がみられた．WMS-Rでは言語性記憶89，視覚性記憶79であるが，遅延再生が70と障害されていた．ウィスコンシンカードソーティングテストでは，カテゴリーは1つも達成されず，保続が認められた．トレールメーキングテスト，ストループテストのパートBでは，同年代の対照に比して延長が認められた．

画像診断：頭部MRIでは，びまん性の脳萎縮に加え，両側脳室周囲の高信号領域を広範に認めた．また基底核にもT$_2$強調，FLAIR画像で高信号を呈するラクナ梗塞を認めた(図1，図2)．脳血流シンチ(IMP)では，小脳および後頭葉の血流は保たれていたが，前頭葉，側頭葉下部において両側とも著明な取込みの低下を認めた．頭頂葉も一次感覚野と帯状回を除き低下して

いた(図3).

補助検査：アポEフェノタイプはE3/E3型であった．アルツハイマー病のバイオマーカーである髄液中のリン酸化タウ蛋白(199Ser)を測定したところ，1.89 fmol/mLと上昇していた(カットオフ値<0.96)[3].

3 考 察

本症例は，以下の考察より脳血管障害を合併したアルツハイマー病と考えられた．脳血管障害として広範な白質病変が認められ，この血管病変が脳機能低下にどの程度寄与しているかを考えることが，血管性痴呆の合併を考えるうえで重要と思われた．

1．アルツハイマー病の診断について

現在一般的に用いられているアルツハイマー病の診断基準はDSM-Ⅳ，ICD-10とNINCDS-ADRDAである．痴呆の診断のあと原因疾患の鑑別診断を行うが，アルツハイマー病の場合はNINCDS-ADRDA基準とDSM-Ⅳ基準が比較的よく一致するため，診断基準の違いは大きな問題とならない．本症例は数年前から活動性の低下があり，易疲労感，頭痛などの不定愁訴が目立っていた．記憶障害の発症時期が不明であり，また経過も緩徐である．CDR 0.5であり，軽度の認知機能障害であるが，神経心理検査で記憶障害(遅延再生)と保続が確認された．抑うつが認知機能に影響を及ぼしている可能性が考えられ，抗うつ薬の投与を行ったが，神経心理検査の成績には改善はみられなかった．脳血管性病変の関与については後述するが，血管障害に伴う局所神経症候は認められなかった．また脳血流シンチで小脳，後頭葉，一次運動知覚野の血流は保たれていたが，両側の側頭葉，頭頂葉を含む広範な低灌流域が認められた．頭頂葉あるいは頭頂葉での脳血流の低下は必ずしもアルツハイマー病を意味するものではないが，本症例では髄液中のリン酸化タウ蛋白が上昇していたことから，アルツハイマー病が強く疑われた．

2．脳血管障害の関与について

血管性痴呆とアルツハイマー病の臨床的な鑑別を目的として，Hachinskiの虚血スコアはしばしば用いられる[4]．Hachinski虚血スコアは，血管性痴呆に多くみられる13項目の症候からなり，7点以上が血管性痴呆，4点以下では変性性痴呆の可能性が高いとされる．本症例では6点であり，やはり

血管障害の関与を考えるうえでは画像所見は必須である．

血管性痴呆の診断には，血管障害と痴呆症状との因果関係が明確であることが重要である．血管性痴呆の診断基準として，DSM-Ⅳ，ICD-10，NINDS-AIREN，ADDTC があるが，これらの基準間の一致率は低い[5]．また DSM-Ⅳ，ADDTC，NINDS-AIREN の順に血管性痴呆と診断される割合が高いとの報告がみられる[6]．DSM-Ⅳでは血管障害の根拠として「障害に病因として関係していると考えられる，局所神経症候もしくは脳血管障害を示す検査所見」とやや漠然とした記載がされており，その判断には熟練を要する．最も厳密な NINDS-AIREN の基準では，血管性痴呆の分類として皮質性血管性痴呆，皮質下性血管性痴呆，Binswanger 病，視床性痴呆が挙げられている．

ここで NINDS-AIREN の診断基準から[7]，本症例を脳血管障害の立場から考えたい．NINDS-AIREN の診断基準(**表1**)では，痴呆の存在に加えて，脳血管障害の存在を示すことが要件である．血管障害の存在は，1)局所神経症候，2)画像所見の両方が必要である．画像所見として，大血管の梗塞や認知機能に枢要な部位の梗塞(strategic 梗塞)，また白質のラクナ，広範な大脳白質病変などの痴呆の発現に関与する脳血管障害が提示されている．本症例では局所神経症候が明らかでなく，血管性痴呆とは考え難い．しかし MRI での広範な脳室周囲白質病変(leukoaraiosis)が認められ，本症例の認知機能の低下に関与している可能性が考えられた．NINDS-AIREN の報告では，血管性痴呆の白質病変の程度について，少なくとも全白質の 1/4 を超える程度が1つの基準として考察されており[7]，本症例ではその意味では十分なサイズと考えられた．また脳室周囲の白質病変は血管性痴呆と考えられる例に認めることが多いが，加齢やアルツハイマー病などの疾患でも認められる所見でもある[8]．アルツハイマー病に認められる脳室周囲白質病変は，病期の進行した例で認められることが多く，血管性痴呆よりも程度が軽度であるとの報告がある[8]．本症例では CDR 0.5 であり軽度の認知障害であるが，血管病変の関与を MRI の画像所見だけで判断することはやはり困難と考えられた．

最近，NINDS-AIREN 診断基準作成グループの一部が皮質下血管性痴呆(subcortical vascular dementia)の基準を作成した[9]．すなわち，**表2**に示すように遂行機能障害と記憶障害(おそらく軽度)の両者を含む認知機能障害，脳画像に関する脳血管障害の証拠および，脳血管障害の証拠となるような神経学的な症候の既存を必須条件に挙げている．NINDS-AIREN の診断基準は，多様な脳血管障害に基づく痴呆を扱うものである．Binswanger 病やラクナ

表1　血管性痴呆の診断基準(NINDS-AIREN 国際ワークショップ)

Ⅰ. probable vascular dementia の診断基準

①痴呆の存在

記憶障害および見当識，集中力，言語，視空間認知，物事の遂行，運動の制御，行為のうち2つ以上の項目での認知機能低下．脳血管障害に伴う身体的影響を除外しても，その認知機能障害により日常生活に支障がある．

②脳血管障害の存在

神経学的検査：局所神経症候(片麻痺，下部顔面神経麻痺，バビンスキー徴候，知覚障害，半盲，構音障害など)．

画像診断：大血管の梗塞，認知機能障害の出現に重要な部位の梗塞(角回，視床，前脳基底部，後大脳動脈領域，前大脳動脈領域など)，基底核の多発梗塞，白質のラクナ，広範な大脳白質病変，あるいはそれらの組み合わせなど痴呆の発現に関与する脳血管障害．

③痴呆の発症と脳血管障害の関連

痴呆の発症が脳卒中発作から3カ月以内である．

認知機能障害が突然発症である，または認知機能障害が変動し，階段状に増悪する．

Ⅱ. probable vascular dementia を支持する臨床所見

(a)初期から歩行障害が認められる．

(b)歩行時の動揺および転倒傾向．

(c)泌尿器疾患によらない頻尿およびその他の排尿障害．

(d)仮性球麻痺．

(e)人格および気分の障害．

Ⅲ. vascular dementia らしくない臨床所見

(a)初期から記憶障害を認め，記憶障害および超皮質性感覚失語，失行，失認などの認知機能障害が，画像所見の変化を伴わずに進行する．

(b)認知機能障害以外の局所神経症状を認めない．

(c)CT や MRI で脳血管障害を認めない．

表2　皮質下血管性痴呆の診断基準(要約)

Ⅰ．A．遂行機能障害と記憶障害(おそらく軽度)の存在と，社会生活活動の以前の水準からの低下．
　　B．以下の両者を含む脳血管障害の存在．すなわち画像診断による関連する脳血管障害の証拠と，神経学的症候の存在あるいは既往．

皮質下血管性痴呆の画像診断
　　A．CT：半卵円中心に達し，少なくとも1つのラクナ梗塞を含む著明な白質病変の存在，および皮質の大梗塞・出血，水頭症や多発性硬化症のような特殊な白質病変の除外．
　　B．MRI
　　1．白質病変優位型：10 mm 以上の PVH，25 mm 以上の連続する白質病変など，または
　　2．ラクナ優位型：基底核領域の5個以上の多発性ラクナと中等度の白質病変および皮質の大梗塞・出血，水頭症や多発性硬化症のような特殊な白質病変の除外．

状態を含む皮質下血管性痴呆のような，穿通枝や髄質動脈の血管障害による血管性痴呆のより明解な診断基準が必要であろう．

3．脳血管障害を合併したアルツハイマー病について

血管性痴呆とアルツハイマー病，あるいは両者の合併について痴呆の原因診断を考えるとき，その判断に苦慮することは決して少ないことではない．血管性痴呆とアルツハイマー病のどちらが，高齢者の脳機能低下の主因であるかを判断できる客観的な方法は現在のところ見当たらない．臨床的な観察を経時的に行うことで，いずれの変化が主因であるかを判断する必要がある．

混合型痴呆については，平井らが詳細な病理学的な検討を行っている[10]．病理学的には混合型痴呆と診断される症例の多くは，アルツハイマー病性病変と脳血管性の病変のいずれもが単独でも痴呆を起こし得る程度に高度であるものであった．しかし平井らは，頻度は低いながら，両者の変化が併存し，それぞれ単独では痴呆を起こすほどの程度ではないが，両者が併存することで痴呆をきたしたものも混合型痴呆に含まれることを報告している[10]．

一方，NINDS-ADRDA の診断基準では，possible AD(痴呆症状があり，痴呆の原因となり得るアルツハイマー病以外の系統的な疾患がなく，発症，症状，経過が定型的でない場合，あるいは痴呆の原因となる他の系統的な疾患が存在するが，現在の痴呆の原因とは考えられない場合)が定義されてい

る[4]．脳血管障害に関しては，血管障害そのものが痴呆の原因と考えられない場合に possible AD と診断する．すなわち，痴呆との因果関係が明確でない脳血管障害を伴う場合は，脳血管障害を伴うアルツハイマー病(possible AD with CVD)と考えるべきであると提唱している[11]．

ここで血管性痴呆とアルツハイマー病の類似性，相違点について簡単に考察したい．痴呆症をきたす疾患で，アルツハイマー病と血管性痴呆が2大疾患であり，それぞれ独立した疾患であることは一般的なコンセンサスであろう．しかし最近の報告では，アルツハイマー病患者の剖検脳の35～50%に血管病変が確認され，また血管性痴呆と診断された患者の45%に tangle の沈着が見られている[1,12]．また脳血管障害とアルツハイマー病の関係を検討した Nun study では，アルツハイマー病と診断された患者で，ラクナ梗塞が基底核部，視床，深部白質に1～2個あると，脳血管障害のない例よりも認知機能も低下していることが指摘されている[12]．これらの結果は，臨床診断からはアルツハイマー病と血管性痴呆として別々に捉えられていた両疾患が，病理的には高頻度に併発しており，また脳血管障害はアルツハイマー病の発症と重症度に相加的に作用している可能性を示している．

また治療の視点から考えると，アルツハイマー病に対しては，ほとんどの症例で塩酸ドネペジルが中心に使用されており，血管性痴呆では，血流改善剤や抗血小板薬の投与，高血圧などの危険因子の管理が中心に行われている．しかし混合型痴呆，または脳血管障害を伴うアルツハイマー病では，どちらの要因が主であるかを判断したうえで，その治療の選択は主治医に委ねられているのが現状と思われる．アルツハイマー病では認知機能は進行性に悪化するのと異なり，血管性痴呆ではリハビリテーションを積極的に行うことで，脳機能はゆっくりと回復することをしばしば経験する．混合型痴呆，あるいは脳血管障害を併発したアルツハイマー病の治療においても，病態に即した幅の広い治療が行われることが望まれる．

4．生活習慣病と痴呆

最後に痴呆の危険因子について，われわれの最近の活動を含めて紹介したい．脳血管障害の最大の危険因子が加齢と高血圧であることは言うまでもない．高血圧は血管性痴呆のみならずアルツハイマー病の危険因子であり，高血圧をコントロールすることでアルツハイマー病の発症を減少できたとする報告もみられる[13]．最近，糖尿病，高脂血症などの高血圧以外の脳血管障害の危険因子も，アルツハイマー病の危険因子でもあることが報告されてい

る[14]．今後これらの危険因子を管理することで，痴呆の発症，また進展が抑制できるかを明らかにすることが重要と思われる．最近，われわれは高齢者糖尿病に着目し，糖尿病コントロールに治療介入を行い，前向きに認知機能の変化を追跡する研究を始めている(高齢者糖尿病を対象とした前向き大規模介入研究：班長多摩老人医療センター院長・井藤英喜先生)．この研究を通じて糖尿病の認知障害に及ぼす影響を明らかにできるものと期待される．

文　献

1) Kalaria RN and Skoog I：Overlap with Alzheimer's disease. Vascular cognitive impairment(Erkinjuntti T and Gauthier S eds), pp145-166, 2002.
2) Itoh N et al：Large-scale, multicenter study of cerebrospinal fluid tau protein phosphorylated at serine 199 for the antemortem diagnosis of Alzheimer's disease. Ann Neurol **50**：150-156, 2001.
3) Toba K et al：Knowledge and utilization of comprehensive geriatric assessment in Japan. Nippon Ronen Igakkai Zasshi **38**：139-147, 2001.
4) アルツハイマー型痴呆の診断，アルツハイマー型痴呆の診断・治療マニュアル(日本老年精神医学会編)，pp43-89，2001.
5) Pohjasvaara T et al：Comparison of different clinical criteria(DSM-Ⅲ, ADDTC, ICD-10, NINDS-AIREN, DSM-Ⅳ)for the diagnosis of vascular dementia. Stroke **31**：2952-2957, 2000.
6) Chui HC et al：Clinical criteria for the diagnosis of vascular dementia；A multicenter study of comparability and interrater reliability. Arch Neurol **57**：191-196, 2000.
7) Roman GC et al：Vascular dementia：diagnostic criteria for research studies. Report of the NINDS-AIREN International Workshop. Neurology **43**：250-260, 1993.
8) Tamotu M et al：Leukoaraiosis in Alzheimer's disease；Clinico-pathological evaluation. Hong Kong J Gerontology **10**：215-218, 1996.
9) Erkinjuntti T et al：Research criteria for subcortical vascular dementia in clinical trials. J Neural Transm Suppl **59**：23-30, 2000.
10) 平井俊策：混合型痴呆問題をめぐって．老年精医誌　**14**：186-192，2003.
11) 北村　伸：アルツハイマー型痴呆と血管性痴呆の境界と相同性をどうとらえるか　どう診断すべきか．　老年精医誌　**14**(増)：70-77，2003.
12) Snowdon DA et al：Brain infarction and the clinical expression of Alzheimer diseases；The Nun Study. JAMA **277**：813-817, 1997.
13) Forette F et al, Systolic Hypertension in Europe Investigators：The prevention of dementia with antihypertensive treatment：new evidence from the Systolic Hypertension in Europe(Syst-Eur) study. Arch Intern Med **162**(18)：2046-2052, 2002.
14) Otto A et al：Diabetes mellitus and the risk of dementia；The Rotterdam study.

Neurology 53：1937-1942, 1999.
15) Pantoni L and Garcia JH：Pathogenesis of leukoaraiosis. Stroke 28：652-659, 1997.
16) Smith CD et al：White matter volumes and periventricular white matter hyperintensities in aging and dementia. Neurology 54：838-842, 2000.
17) 山崎峰雄ほか：ビンスワンガー型痴呆の成因．老年精医誌 14：193-192, 197, 2003.
18) Schmidt R et al：MRI white matter hyperintensities－three years follow up of the Austrian Stroke Prevention Study－. Neurology 53：132-139, 1999.

質疑応答

座長
◎難波　吉雄(東京大学医学部老年病科)
演者
◎櫻井　孝(神戸大学医学部老年内科)
天野　隆弘(慶應義塾大学医学部神経内科)
北村　伸(日本医科大学附属第二病院内科)
(発言順)

難波　どうもありがとうございました．血管性痴呆とアルツハイマー型痴呆のオーバーラップということで，実際ご経験された症例を含め，ディスカッションをお願いいたします．

■白質病変があるか

天野(隆)　先生はいま血管性痴呆とアルツハイマー病の合併ということで苦慮されていると思います．私も約1年前に，28例の3～4年追跡したアルツハイマー病症例で，とくにFLAIR法で白質病変があるかどうかを検討しました．Fazekasの重症度分類による白質病変の重症度2，3度が22%に認められました．ですから，このような白質変化を血管性痴呆によるものと診断すると，結局アルツハイマー型痴呆(AD)＋血管性痴呆になってしまうと思います．

ADもわれわれが思っている以上に，白質病変がよくみつかるのです．私の印象としては，アルツハイマー病症例は経過を追ってMRIを行うと白質病変の出現が多くなり，血管性痴呆の合併と診断しない方がよいと思っています．

ただ先生の場合は，痴呆の検査で22点ですね．ADASで7点くらいで痴呆の程度がひどくないのに，大きい虚血性変化があるので，悩んでおられると思うのです．

この白質病変については以前から興味があっていろいろ検討していますが，一方，外来でこの程度の白質病変がありながら何も症状がないという方が時にいらっしゃいますね．そういう症例に痴呆があれば，Binswanger病と診断してしまうことになると思います．

白質の変化が著しくありながら，たとえば銀行のエリートコースを歩んで

いる方もありました．画像では同じような感じの方がしばしば発見されます．そうすると，画像による白質病変だけでこの病変イコール痴呆の原因だと診断すると間違ってしまうのではないかと思っているのですが，その点はいかがでしょうか．

櫻井　まさしくおっしゃる通りだと思います．ただこの症例ではMRIで比較的広範な白質病変があり，SPECTで前頭葉にも少なからず脳血流の低下がみられました．そこで白質の虚血性病変が認知機能に関与している可能性を考えました．

■アルツハイマー型痴呆とする根拠

北村　血管性痴呆とするには痴呆と関連する脳血管障害が病歴と画像であるということが大切だと思うのですが，この例は病歴にはなく，神経症候もありません．画像上は血管病変を思わせるものがありますが，やはり血管性痴呆と診断するのはちょっと難しい，徐々に悪化していることを考えると，やはりアルツハイマー型痴呆は否定できないという印象です．それからアルツハイマー型痴呆でもSPECTで前頭葉の血流が低下していることはありますから，アルツハイマー型痴呆と考えてよいかなと思います．

もう1つは，3DSSPでのSPECTの解析で，後部帯状回の低下があると，アルツハイマー型痴呆の1つの証拠になる可能性があると思います．

また，私がこのような例で血管性痴呆ではないかと疑って剖検を行ったら，老人斑がなく神経原線維変化だけが多く，dementia of the neurofibrillary tangle typeで，そうするとタウノパチーと一致するという症例を経験していますので，コメントさせていただきました．

櫻井　ありがとうございます．

難波　どうもありがとうございました．

Imaging of Fine Structure of Bone Sample with High Coherent X-ray Beam and High Spatial Resolution Detector

Masatsugu Hirano, Katsuhito Yamasaki, Riko Kitazawa, Sohei Kitazawa, Hiroshi Okada, Tetsuro Katafuchi, Takashi Sakurai, Takeshi Kondoh, Chiho Ohbayashi, Sakan Maeda, Kazuro Sugimura, and Shinichi Tamura

Reprinted from Radiation Medicine Vol. 22 No. 1
January - February 2004

TECHNICAL NOTE

Radiation Medicine: Vol. 22 No. 1, 56–59 p.p., 2004

Imaging of Fine Structure of Bone Sample with High Coherent X-ray Beam and High Spatial Resolution Detector

Masatsugu Hirano,[1] Katsuhito Yamasaki,[2] Riko Kitazawa,[3] Sohei Kitazawa,[3] Hiroshi Okada,[4] Tetsuro Katafuchi,[9] Takashi Sakurai,[5] Takeshi Kondoh,[6] Chiho Ohbayashi,[8] Sakan Maeda,[3] Kazuro Sugimura,[7] and Shinichi Tamura[1]

In this study, we observed bone specimens of the mouse using a very high coherence beam and high spatial resolution detector (zooming tube: approximately 0.7 micron resolution) and successfully obtained images of the Haversian canal, osteocytes, and osteoclasts.

Key words: X-ray imaging, synchrotron radiation, high spatial resolution, Haversian canal, osteocyte, osteoclast

Introduction

Although the technology of X-ray diagnostic equipment has improved markedly, conventional absorption imaging is limited in that its application to the observation of objects with small absorption rates is difficult. Expectations are mounting for the development and realization of a next-generation coherent X-ray source similar to that of the laser. Refraction contrast by X-rays (synchrotron radiation) of such high coherence would enable higher contrast imaging, which would reflect object density differently than the absorption imaging method.[1] Radiation dose can be reduced and spatial resolution can be improved using synchrotron radiation X-rays.[2,3] Thus, there is potential for clinical application to detect breast cancer.[4] Refraction contrast imaging by generating bright and dark lines on the object interface[5] has the effect of improving visibility.[3,6] Further, phase contrast CT has been developed by Momose *et al.*[7] It has been impossible to obtain such images with conventional radiation sources owing to their low degree of coherence. However, third-generation radiation sources have provided highly coherent imaging. Contrast imaging can be applied to the fields of orthopedics, breast cancer, and respiratory systems, among others. This success is due to the high spatial resolution detector and well-collimated X-ray beam.

Materials and Methods

This experiment was performed with a RIKEN Coherent X-ray Optics beam line (BL29XU at SPring-8). The schema of the set-up is shown in Fig. 1. The X-ray detector was zooming tube C5333 (Hamamatsu Photonics K.K., Shizuoka, Japan). The measured spatial resolution of the detector was 0.7 μm at 8 keV.[8] The X-ray energy was set at 12.4 keV by a monochromator in this experiment. The sample was placed at a distance of about 990 m downstream of the slit and 1.6 m upstream of the detector. The coherence length was approximately 200 μm. For example, the spatial coherence length of Photon Factory (PF BL-14C), a second-generation facility of synchrotron radiation, is 11 μm.[9]

Resected fibula of mouse (diameter, 300 μm) was used as a specimen to avoid overlapping of bone tissue and provide clear observation.

X-ray flux in front of the sample was measured at about 1.5×10^{11} photon/sec by ion-chamber, and beam exposure time was 20 sec. Therefore the radiation dose was estimated at about 18 Gy.

Received August 5, 2003; revision accepted November 1, 2003.

[1]Division of Interdisciplinary Image Analysis, Osaka University Graduate School of Medicine

[2]Japan Synchrotron Radiation Research Institute

Departments of [3]Pathology, [4]Urology, [5]Internal and Geriatric Medicine, [6]Neurosurgery, and [7]Radiology, Kobe University Graduate School of Medicine

[8]Department of Pathology, Kobe University Hospital

[9]National Cardiovascular Center

Reprint requests to Masatsugu Hirano, Interdisciplinary Image Analysis, Osaka University Graduate School of Medicine, D11, 2-2 Yamadaoka, Osaka 565-0871, JAPAN.

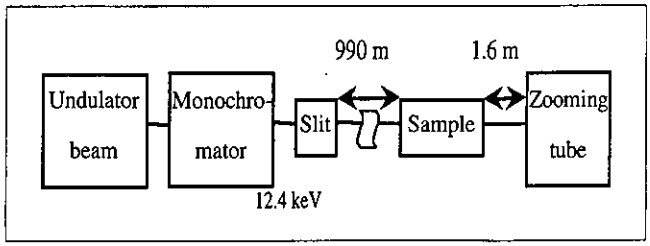

Fig. 1. Schema of set-up.

Results

The reference image of the sample placed about 1 m downstream of the slit and about 2 m upstream of the 6 μm pixel size detector at the SPring-8 bending-magnet beamline is shown in Fig. 2. The same sample was imaged with high resolution at BL29XU (Fig. 3). Tube structure was observed in the center of the tissue. Measured diameter was 30-40 μm. This was assumed to be the Haversian canal. The cecal tube was connected to the Haversian canal. A cell-like structure with a multiangular margin observed at the end of the cecal tube was assumed to be an osteoclast. A fine tubular structure observed parallel to the Haversian canal was assumed to be a small blood vessel or canaliculus. The diameter of the fine tube was about 3 μm, and a spindle structure observed around it was assumed to be an osteocyte. These were 20-40 μm in size. The measured sizes of structures are compared with those of reference10 in Table 1. Sizes are smaller than those of the adult human because the sample was from a mouse fetus. These are the world's first radiographic images of fine structures of bone obtained using a high coherence X-ray beam with high spatial resolution.

Discussion

Using beamline BL20B2 at SPring-8, Mori *et al.* investigated bone samples with mammography film whose spatial resolution was a few microns.[9] Our imaging was done with a detector whose spatial resolution was 0.7 microns. The measured size of osteocytes and osteoclasts was more than 10 μm, and imaging was performed adequately.

This beam can be regarded as a parallel beam. The size of the field view in Fig. 3a is about 300 μm, almost equivalent to the coherence length. This means that the field view has very high coherence, and the coherence improves the contrast and produces high visibility owing to the refraction effect of X-rays at the object's boundary. A bright line was observed inside the Haversian canal and a dark line outside it. Such pairs of lines originated from the refraction of X-rays. Refraction occurred at

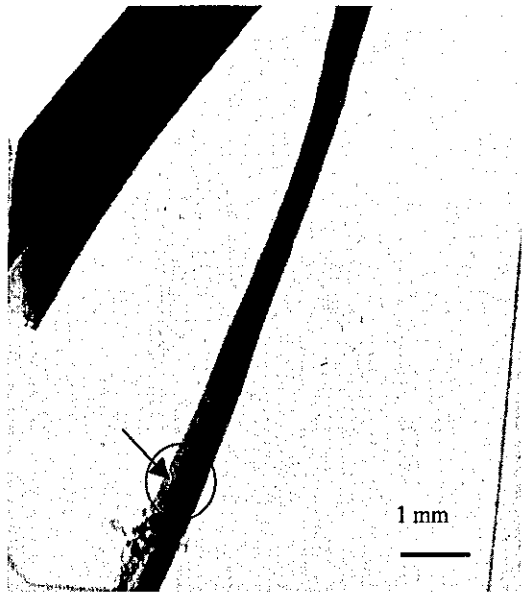

Fig. 2. Overview image of bone sample obtained with the bending magnet beamline.

the wall of the Haversian canal. The ray-tracing method simulated this refraction. The diameter of tube was 30 μm, and the densities in and outside the tube were assumed to be 1.0 and 1.7, respectively. Experimental and simulated images of the Haversian canal are shown in Fig. 5a and 5b, respectively. Profile curves of X-ray intensity are shown in Fig. 5c. The slope of the outside of the Haversian canal was smaller than the simulated slope. This means that density transition is low at the wall of the Haversian canal. Figure 6a shows a canaliculus, small blood vessel, osteocyte, and trabecula. These structures are periodic and parallel to the Haversian canal. Figure 6b shows a profile curve along the line in Fig. 6a. This curve shows periodic structure. Figure 6c shows the auto-correlation function of this profile curve. The auto-correlation function revealed the periodic pattern of these structures. Although speckles are sometimes observed using coherent X-ray imaging, our measurement showed no random speckles. However, it is possible that non-random pattern speckles are able to exist. There is no physical method to distinguish non-random speckles and the radiographic pattern of anatomical fine structure. The only method of distinguishing them is diagnostic observation by a radiologist.

Conclusion

In this study, fine structure of bone was successfully observed using high coherence X-rays. Contrast was improved incredibly using high coherence X-rays. Bone imaging can be performed using a light microscope or electron microscope, but many structures are destroyed

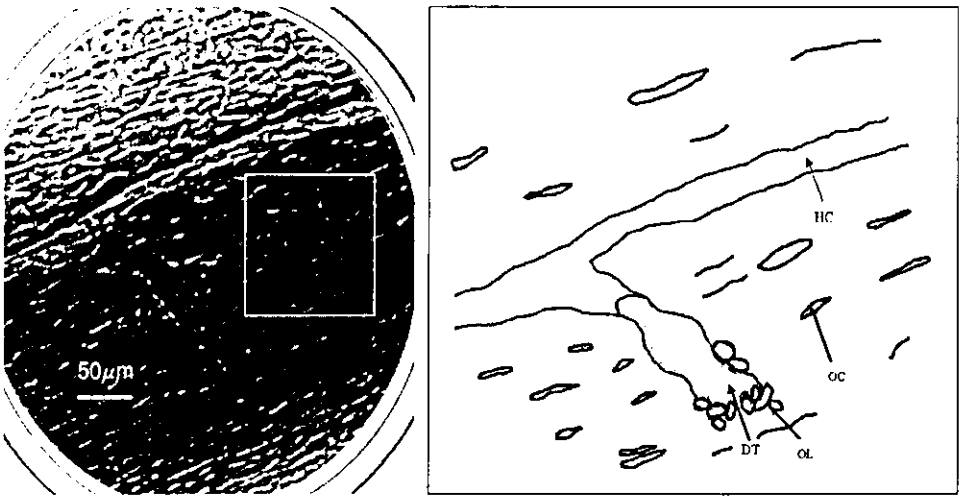

a | b

Fig. 3. a: Magnified image of Fig. 2 (circle) with coherent X-ray optics beam line.
b: Schema of Fig. 3a. Haversian canal (HC), osteocyte (OC), osteoclast (OL), and tunnel in bone tissue (DT) are shown.

Table 1. Diameters of the Haversian canal, osteocytes, and osteoclast measured in this experiment compared with those of adult human in reference 10

	Diameter of Haversian canal (μm)	Osteocytes (μm)	Osteoclasts (μm)
Experimental data	30-40	20-40	10-20
Data from reference	ca. 70	10-50	30-80

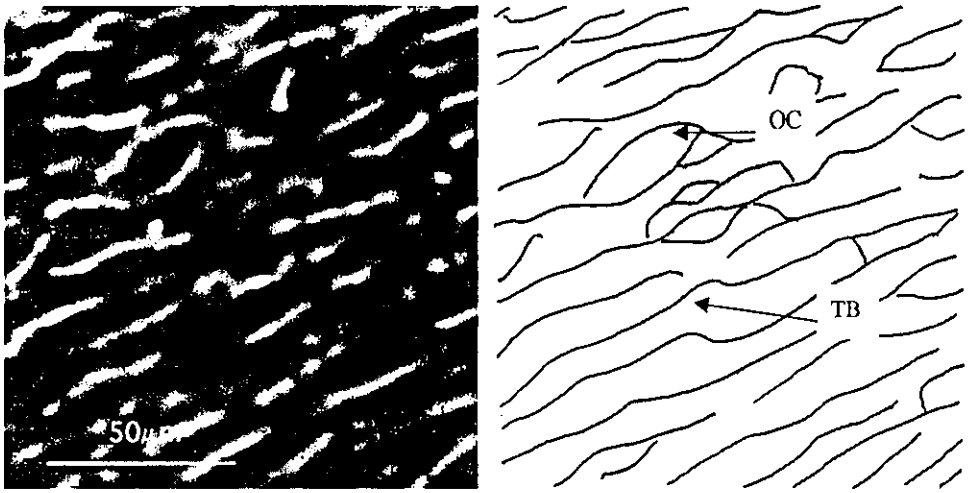

a | b

Fig. 4. a: Magnified image of Fig. 3 (rectangle). Trabecula is easily observed.
b: Schema of Fig. 4a. Osteocyte (OC) and trabecula (TB) are shown.

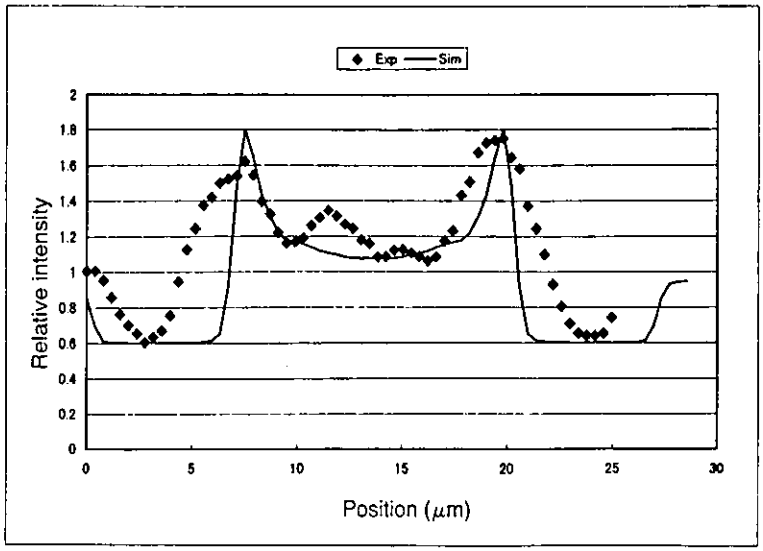

c | a / b

Fig. 5. a: Experimental image of Haversian canal.
b: Simulated image.
c: Profile curves of experimental and simulated images.

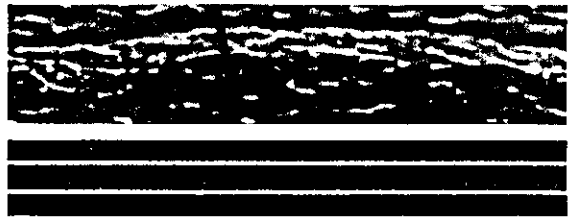

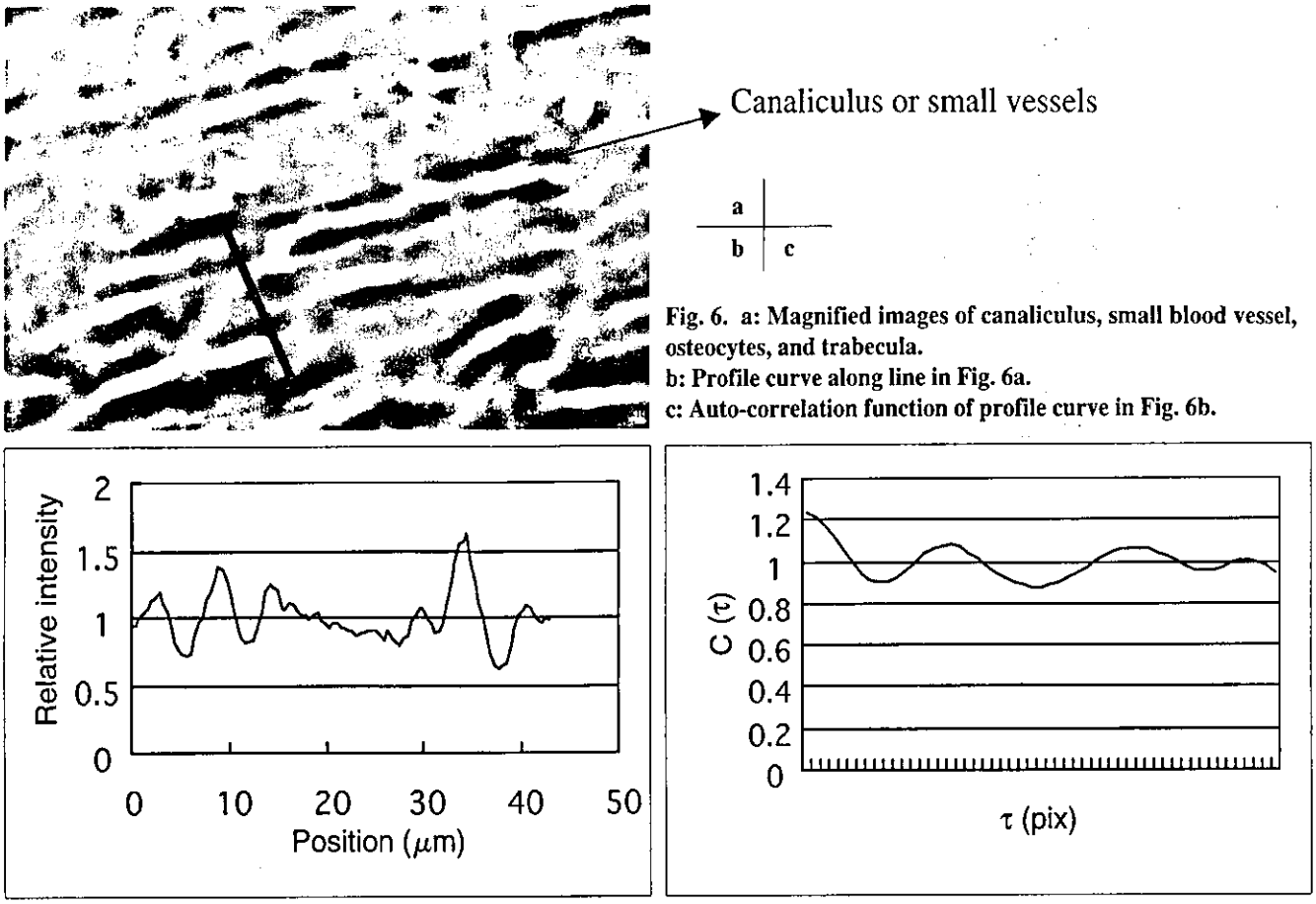

Fig. 6. a: Magnified images of canaliculus, small blood vessel, osteocytes, and trabecula.
b: Profile curve along line in Fig. 6a.
c: Auto-correlation function of profile curve in Fig. 6b.

by preparing samples. There is minimal sample destruction in X-ray microscopic imaging, and the potential exists to observe the fine structure of thin living bone tissue using high coherence X-rays.

Acknowledgments

The authors would like to thank Dr. Masami Ando and Dr. Yoshiki Kohmura for helpful discussions. This study was partly funded by a research grant (No. 14570899) from the Ministry of Education, Culture, Sports, Science and Technology.

References

1) Snigirev A, Snigireva I, Kohn V, Kuznetsov S, Schelokov I. On the possibilities of x-ray phase contrast microimaging by coherent high-energy synchrotron radiation. *Rev Sci Instrum,* 66: 5486–5492, 1995.
2) Hirano M, Yamasaki K, Nagai H, *et al.* Radiation dose and spatial resolution evaluation in SR imaging. In *Proc. Workshop on Medical Applications of Synchrotron Radiation,* ESRF, p. 54, 2001.
3) Hirano M, Yamasaki K, Nagai H, *et al.* Refraction-enhanced X-ray imaging of 10 m distance using synchrotron radiation source. In *Proc. of Joint Symposium on Bio-Sensing and Bio-Imaging,* 1B-8: pp. 128–129, 2001.
4) Alfelli F, Bonvicini V, Bravin A, *et al.* Mammography with synchrotron radiation: phase-detection techniques. *Radiology,* 215: 286–293, 2000.
5) Yagi N, Suzuki Y, Umetani K, *et al.* Refraction-enhanced x-ray imaging of mouse lung using synchrotron radiation source. *Med Phys,* 26: 2190–2193, 1999.
6) Kono M, Obayashi C, Yamasaki K, *et al.* Refraction imaging and histologic correlation in excised tissue from a normal human lung. *Acad Radiol,* 8: 898–902, 2001.
7) Momose A, Takeda T, Itai Y, Yoneyama A, Hirano K. Perspective for medical applications of phase-contrast X-ray imaging. In *Medical Applications of Synchrotron Radiation,* (Ando M, Uyama C eds.; Springer-Verlag, Tokyo), pp. 54–62, 1998.
8) Takano H, Suzuki Y, Uesugi K, Takeuchi A, Yagi N. Point spread function measurement of imaging detectors with an x-ray microbeam. In *Proc. of the SPIE Conference,* 4499: p.126, 2001.
9) Mori K, Sekine N, Sato H, *et al.* Development of phase contrast radiography for bone imaging using synchrotron radiation. *Anal Sci,* 17: i1427–1430, 2001.
10) Harris J. Histology: the lives and death of cells in tissues. In *Molecular Biology of the Cell, 4th ed.* (Alberts B, Bray D eds.; Garland Science, NY), p. 1306, 2002.

Available online at www.sciencedirect.com
SCIENCE DIRECT
Neuroscience Research 50 (2004) 467–474
Neuroscience Research
www.elsevier.com/locate/neures

Glycolysis regulates the induction of lactate utilization for synaptic potentials after hypoxia in the granule cell of guinea pig hippocampus

Toshihiro Takata[a,*], Bo Yang[a], Takashi Sakurai[a], Yasuhiro Okada[b], Koichi Yokono[a]

[a]*Department of Internal and Geriatric Medicine, Kobe University Graduate School of Medicine, 7-5-1 Kusunoki-cho, Chuo-ku, Kobe 650-0017, Japan*
[b]*Health Sciences Center, Kobe Health-Life Plaza, 5-1-2-300, Hyogo-ku, Kobe, Japan*

Received 9 June 2004; accepted 19 August 2004
Available online 21 September 2004

Abstract

Lactate is considered an alternative substrate that is capable of replacing glucose in maintaining synaptic function in adult neurons. But, we found recently that lactate could be utilized for maintenance of synaptic potentials only after the activation of NMDA and voltage-dependent-calcium channel during glucose deprivation. To clarify more on the relationship between glycolysis and induction of lactate utilization, we tested lower concentration of glucose with hypoxia to induce a relative shortage of anaerobic energy production. Population spikes are not maintained with lactate following hypoxia in 10 mM glucose medium, but are maintained at their original levels with lactate after exposure to hypoxia in lower concentration (5 mM) of glucose. Hypothermia during low glucose-hypoxia, bath application of the NMDA channel blocker and the voltage-sensitive calcium channel blocker, as well as the omission of extracellular calcium prevented the induction of the lactate-supported population spikes. ATP levels in the tissue slices are relatively preserved in the conditions that block the induction of lactate-supported population spikes. From these observations, we propose that the energy source for maintenance of synaptic function in adult neuron changes from adult form (glucose alone) to immature one (glucose and/or lactate) after short of glucose supply.

Keywords: Glycolysis; Lactate; Field potential; NMDA receptor; Voltage-sensitive calcium channel; Adenosine triphosphate; Glutamate release

1. Introduction

It is well known that lactate can be utilized as an energy substrate instead of glucose in the immature brain (Wada et al., 1997) and that it can also be used to maintain the energy level of the mature brain (Saitoh et al., 1994; Kanatani et al., 1995; Wada et al., 1998). Under ordinary conditions, glucose is the primary substrate in the brain for the maintenance of basic synaptic activity (Cox and Bachelard, 1988; Takata and Okada, 1995; Dienel and Hertz, 2001) and for providing energy to maintain the activated state (Fox et al., 1988; Roberts, 1993; Chih et al., 2001a,b). However, the role of lactate in the maintenance of synaptic function in the adult brain is controversial (Schurr, 1988; Fowler, 1993; Takata and Okada, 1995; Izumi et al., 1997; Takata et al., 2001; Dienel and Hertz, 2001). In rapidly prepared hippocampal slices (which are supposed to yield less damaged neurons; Yamane et al., 2000), synaptic potentials cannot be preserved in circulating medium containing lactate instead of glucose (Saitoh et al., 1994; Takata and Okada, 1995; Yamane et al., 2000; Takata et al., 2001). Synaptic potentials can, however, be well-maintained in lactate medium after the slices have undergone glucose deprivation or if the hippocampus slices are prepared slowly under condition thought to mimic ischemia (Sakurai et al., 2000; Yamane et al., 2000). In addition, synaptic potentials recorded at reduced temperature (e.g., 30 °C; Izumi et al., 1997, 29 °C; Takata et al., 1997) show dramatic resistance to glucose deprivation, suggesting that mild hypothermia itself covers the significant role of anaerobic glycolysis for maintenance of the synaptic potential at higher physiological temperature (Takata et al., 1997). Therefore, the results of the experiments conducted at reduced temperature require careful interpretation, especially when they are related to metabolic processes such as glycolysis. These results

* Corresponding author. Tel.: +81 78 382 5901; fax: +81 78 382 5919.
E-mail address: takata-tky@umin.ac.jp (T. Takata).

0168-0102/$ – see front matter © 2004 Published by Elsevier Ireland Ltd and the Japan Neuroscience Society.
doi:10.1016/j.neures.2004.08.008

suggest that lactate can support synaptic potentials under conditions similar to post-insult states or in a protective environment such as hypothermia.

We have demonstrated that the population spikes (PS) in the dentate gyrus (DG) of the hippocampus spontaneously recover after transient suppression during lactate replacement for glucose (Saitoh et al., 1994; Takata et al., 2001). This phenomenon is dependent upon activation of *N*-methyl-D-aspartate (NMDA) receptors and voltage-sensitive calcium channels (VSCCs; Takata et al., 2001). We have proposed that lactate will only be efficiently utilized for the maintenance of synaptic potentials after a trigger event that induces Ca^{2+} influx, such as hypoglycemia or other cytotoxic insults (Takata et al., 2001). With regard to energy metabolism in the neuron, we hypothesize that synaptic function is maintained by both anaerobic glycolysis and mitochondrial oxidation, and that anaerobic glycolysis plays an essential role in the maintenance of synaptic potentials in spite of its minor contribution towards energy production (Takata and Okada, 1995; Yamane et al., 2000; Takata et al., 2001). Furthermore, energy utilization for synaptic function may be regulated via a mechanism which involves switching from anaerobic to aerobic glycolysis in response to Ca^{2+} influx. To better understand the switching mechanism enabling the use of lactate for maintaining synaptic potentials, we analyzed the effect of hypoxia on lactate utilization for maintenance of PS under conditions of varying glucose concentrations. Under these conditions, enhanced glycolysis (a Pasteur effect) induced by hypoxia highlights the role of anaerobic glycolysis for the induction of lactate utilization to maintain synaptic potentials. The introduction of hypothermia during hypoxia was employed to examine the utilization of lactate for synaptic potential maintenance under conditions in which glucose consumption is relatively spared. In conjunction with the electrophysiological study, we also examined the levels of ATP and extracellular glutamate in the hippocampal slices during hypoxia under varying glucose conditions.

2. Materials and methods

2.1. Preparation of hippocampal slices

Adult guinea pigs (Hartley, SLC, Japan), weighing 200–300 g, were sacrificed according to the guidelines for animal experimentation at the Kobe University School of Medicine. Hippocampus slices (300–400 μm) were prepared by cutting transversely along the long axis of the hippocampus as described (Okada, 1988). Each slice was preincubated for 20 min in the standard medium (in mM: NaCl 125, KCl 4, KH_2PO_4 1.24, $MgSO_4$ 1.3, $CaCl_2$ 2, $NaHCO_3$ 26, glucose 10) bubbled with 95% O_2 and 5% CO_2 at 35 °C and was kept at room temperature until usage. For the experiment of reduced level of glucose during hypoxia, we chose 5 mM because it is the critical level that the population spikes can be recorded stably from hippocampal slice (Li et al., 2000).

2.2. Electrical activity recording

After preincubation, each slice was transferred to an observation chamber equipped with a stereoscope. The chamber was perfused continuously with the standard medium at a flow rate of 4 ml/min. With this perfusion speed, the medium in recording chamber is replaced in 3 min. The temperature was maintained at 35 °C throughout the experiment with an incubator and temperature controller (PDMI-2, Medical Systems Corp., NY). The temperature of the incubator was continuously monitored and with this system, hypothermia from 35 to 30 °C can be achieved within 3 min. As an index of neural activity, the perforant path was stimulated at 0.1 Hz with constant current pulses (0.1 ms) and population spikes (PS) were recorded from the granule cell layer of the dentate gyrus (DG) with glass microelectrodes filled with 2 M NaCl. The stimulation intensity was adjusted to obtain PS amplitudes at 60–70% of the maximum elicited by supramaximal stimulation. After recording steady potentials for at least 20 min, the slices were perfused with conditioned medium. Hypoxia was introduced by switching to the perfusion medium bubbled with 95% N_2/5% CO_2. To test the effects of lactate during deprivation of glucose, glucose in the medium was replaced with 10 mM sodium lactate (lactate medium). Adding sodium lactate did not influence the pH of the medium.

2.3. ATP determination

DG regions were dissected from hippocampal slices under a stereoscope. After preincubation for 20 min in oxygenated standard medium at 35 °C, the dissected slices were incubated for 10 min in either standard medium (10 mM glucose), 5 mM glucose medium or hypoxic glucose-free medium bubbled with 95% N_2/5% CO_2. At the end of the incubation, the DG regions of four slices were immediately homogenized in 0.5 N perchloric acid with 1 mM ethylenediaminetetraacetic acid (EDTA) and centrifuged for 15 min at 2000 rpm. The supernatant was neutralized with 2 M $KHCO_3$, recentrifuged and stored at −30 °C until assay of ATP. ATP was quantitated enzymatically and fluorometrically by measuring the production of nicotinamide adenine dinucleotide phosphate hydride (NADPH; Okada, 1974). Protein content of the slices was determined by the method of Lowry and Passonneau (1951).

2.4. Determination of glutamate release

After preincubation (see above), 4–5 DG slices were incubated for another 20 min in 300 μl of standard medium bubbled with 95% O_2/5% CO_2 at 35 °C and the basal level of glutamate in the medium was determined. Hypoxia experiments were performed using medium bubbled with

95% N_2/5% CO_2. The concentration of glucose in the medium was either 0, 5, or 10 mM. After incubation in each medium, the quantity of glutamate released from the slices was determined by high performance liquid chromatography (HPLC). Prior to chromatography, the medium was filtered through 0.22 μm Millipore filters. Aliquoted medium (6 μl) was injected into vials and placed in a refrigerated automicrosampler (CMA/200, CMA, Stockholm). Samples were mixed with reagents, applied to a reverse-phase column (BAS, Tokyo), and the column eluate was monitored with a fluorescence detector (CMA/280, CMA, Stockholm). Analyzed data were printed out with a chromatographic recorder (D-2500, Hitachi, Tokyo). Sample concentrations were calculated using chromatograms generated with known concentrations of amino acid standards.

2.5. Materials

ATP, protein assay reagents, nimodipine and D-(-)-2-amino-5-phosphonovaleric acid (APV) were purchased from Nacalai Co., Japan. Hexokinase, glucose-6-phosphatedehydrogenase (G6PDH) and all other enzymes were obtained from Boehringer Mannheim, Germany. Sodium lactate was obtained from Sigma, U.S.A.

2.6. Statistical analysis

Values are shown as mean ± S.E.M. Statistical analysis was performed by ANOVA and Bonferroni post hoc test and paired *t*-test. Treatment differences were considered significant at $P < 0.05$.

3. Results

3.1. The induction of lactate-supported PS is dependent on glucose and the activation of NMDA/VSCC

The time course of PS during hypoxia for 10 min and subsequent replacement of glucose with lactate is shown in Fig. 1. The amplitude of PS rapidly declines in a similar manner during hypoxia in medium containing 5 or 10 mM glucose. Surprisingly, the PS amplitude is maintained after replacement of lactate for glucose when the glucose content during hypoxia exposure is 5 mM while it is transiently reduced and subsequently recovers in the 10 mM glucose medium (Fig. 1).

We previously demonstrated that the transient block and subsequent recovery of synaptic potentials in the DG of the hippocampus after replacement of lactate for glucose is dependent on the activation of NMDA receptors and VSCCs (Takata et al., 2001). Thus, we next studied the effect of the NMDA receptor antagonist, APV, and the VSCC antagonist, nimodipine, on the induction of lactate-supported PS after exposure to low glucose and hypoxia. During hypoxia with 5 mM glucose medium, 50 μM both APV and nimodipine

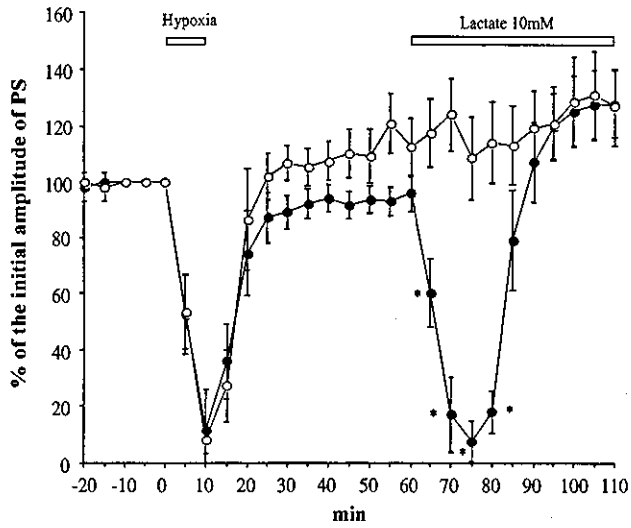

Fig. 1. Time course of the change in the amplitude of population spikes after exposure to hypoxia using 5 mM (open circles) or 10 mM glucose (filled circles) in the perfusion medium. Hypoxia was introduced for 10 min and glucose was replaced with 10 mM lactate in the perfusion medium after recovery from hypoxia exposure as indicated by the open horizontal bars. The ordinate is the percent of the initial amplitude of population spikes recorded from the granule cell layer of hippocampal dentate gyrus. Each plot indicates the mean value ± S.E.M. of five slices. Asterisks indicate a significant difference in amplitude between 5 and 10 mM glucose conditions.

were applied to the perfusion medium. Under these conditions, the PS amplitude is not maintained following lactate substitution and shows a transient block with subsequent recovery similar to that observed with the medium containing 10 mM glucose in the original experiment (Fig. 2). This result suggests that the induction of lactate-supported PS after hypoxia with the lower glucose level is also dependent on the activation of NMDA receptors

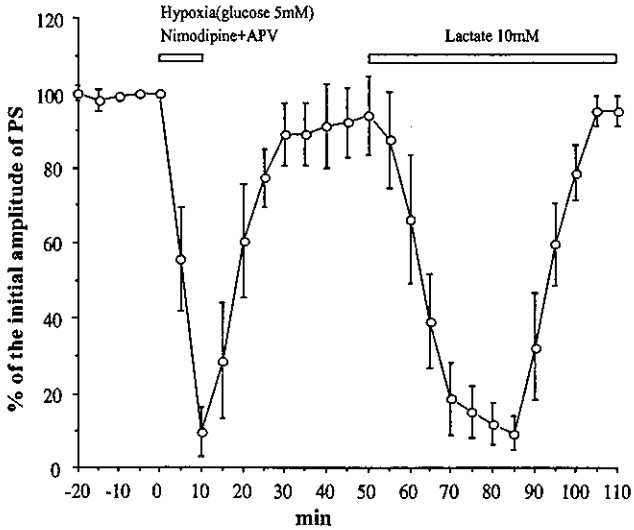

Fig. 2. Effect of APV and nimodipine on the change in amplitude of population spikes during subsequent replacement of glucose with lactate. The NMDA receptor antagonist, APV, and voltage-sensitive calcium channel antagonist, nimodipine, were included in the perfusion medium containing 5 mM glucose during hypoxia as indicated by the horizontal bars. The ordinate is the same as in Fig. 1. Each plot indicates the mean value ± S.E.M. of five slices.

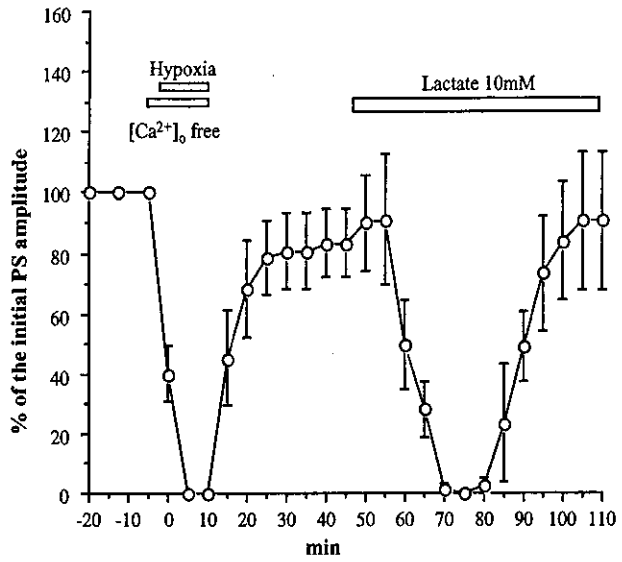

Fig. 3. Effect of the omission of extracellular calcium during hypoxia on the amplitude of population spikes during subsequent replacement of glucose with lactate. Calcium was omitted from the perfusion medium containing 5 mM glucose and 200 μM EGTA was added (to remove any free Ca^{2+}) 5 min before start of hypoxia as indicated by open horizontal bars. Zero minute on the horizontal axis indicates the start time of hypoxia. After recovery of PS amplitude, the perfusion medium was replaced with glucose-free medium containing 10 mM lactate as shown. The ordinate is the same as in Fig. 1. Each plot indicates the mean value ±S.E.M. of five slices.

and VSCCs. We did not observe the same phenomenon after ischemia-like conditions (hypoxia and glucose-free medium); recovery from such a severe challenge is rare (data not shown).

To further elucidate the role of Ca^{2+} influx through the NMDA receptor and VSCCs, slices were subjected to hypoxia with 5 mM glucose, but no Ca^{2+} in the perfusion medium (Fig. 3). The time course of the PS amplitude exhibits a transient block of PS with recovery during lactate replacement for glucose, indicating that the effect of the low glucose level seen in Fig. 1 is negated without extracellular calcium. The level of 5 mM glucose itself is sufficient for maintenance of PS in the dentate gyrus of hippocampus (Kanatani et al., 1995; Li et al., 2000). These results demonstrate that the induction of lactate-supported PS is dependent on Ca^{2+} influx through the NMDA receptor and the VSCC, and that the small reduction of glucose levels (from 10 to 5 mM), which does not influence the basic PS amplitude, triggers the activation of these channels during hypoxia.

3.2. Hypothermia can prevent the induction of lactate utilization for PS

Mild hypothermia (33–29 °C) drastically reduces Ca^{2+} accumulation in the cell and improves the recovery of PS after oxygen and/or glucose deprivation (Takata et al., 1997). Furthermore, we previously reported that hypothermia prevented the decline of PS and ATP levels in the slices, particularly during glucose deprivation. These results suggest that a component of the mechanism used to sustain PS and ATP levels by anaerobic glycolysis is highly temperature sensitive (Takata et al., 1997). Based on these observations, we proposed that hypothermia will prevent the reduction of ATP levels that may trigger the activation of the NMDA receptor and the VSCC. First, we tested the effect of hypothermia on PS amplitude in lactate medium at 30 °C. Upon lowering the temperature to 30 °C with 10 mM glucose, an initial mild transient depression (80% of the initial amplitude) of PS is observed, after which the amplitude rises to 120% (Fig. 4A). The temperature of 30 °C was chosen because a previous report by Aihara et al. (2001) showed that, within the range of 17–36 °C, 30 °C resulted in PS with the highest amplitude. Indeed, the degree of increase of PS in our experiments is almost identical with their results. By selecting the temperature at which the amplitude of PS is maximized, we can see easily the response in PS when there is a depressive effect from energy deprivation. Next, lactate was introduced and the amplitude of PS initially increased to 140% and subsequently stabilized at 120–130% (Fig. 4A). This result confirms that lactate can maintain synaptic potentials at 30 °C for at least 60 min as in the case of glucose deprivation with hypothermia. When hypothermia is introduced during hypoxia with 5 mM glucose in the perfusion medium, the PS amplitude is reduced to 60% and recovers fully after recirculation of standard oxygenated medium at 35 °C. After replacement of glucose with lactate, a transient blockade and subsequent spontaneous recovery of PS results (Fig. 4B). This suggests that hypothermia prevents the exhaustion of energy originating from anaerobic glycolysis and maintains the essential energy levels that prohibit the induction of lactate-supported synaptic potentials.

3.3. ATP levels in the DG region

Lowering the glucose levels in the medium during hypoxia enables PS to be maintained at the original levels in the lactate medium, however, hypothermia prevents this maintenance effect. We next determined the energy (i.e., ATP) levels in the slices under both conditions. The DG region of each slice was selectively dissected and incubated for 10 min in standard medium (containing 10 mM glucose), glucose-free medium (ischemia-like conditions), or 5 mM glucose medium bubbled with 95% N_2/5% CO_2 (hypoxic conditions). The ATP concentration of each sample was determined by a sensitive microassay method (Okada, 1974). ATP levels in the slices are 13.6 ± 0.55 mmol/kg protein under the control conditions (10 mM glucose bubbled with 95% O_2/5% CO_2). ATP levels were reduced in each experimental case relative to the control. The ATP level was 12.8% of the control level under ischemia-like conditions, 36% of the control in 5 mM glucose medium with hypoxia, and 66.6% of the control in 10 mM glucose medium with hypoxia (Fig. 5). When hypothermia is introduced with the 5 mM glucose-containing medium, the